

# SOL parallel momentum loss in ASDEX Upgrade and comparison with SOLPS



I. Paradel Pérez<sup>a,b,\*</sup>, A. Scarabosio<sup>b</sup>, M. Groth<sup>a</sup>, M. Wischmeier<sup>b</sup>, F. Reimold<sup>c</sup>,  
ASDEX Upgrade Team<sup>b</sup>

<sup>a</sup>Aalto University, Department of Applied Physics, Otakaari 1, 02150 Espoo, Finland

<sup>b</sup>Max-Planck-Institut für Plasmaphysik, 85748 Garching, Germany

<sup>c</sup>Forschungszentrum Jülich GmbH, 52425 Jülich, Germany

## ARTICLE INFO

### Article history:

Received 15 July 2016

Revised 5 January 2017

Accepted 22 January 2017

Available online 23 March 2017

### Keywords:

Momentum removal

Scrape-off layer

SOLPS

Divertor detachment

## ABSTRACT

An H-mode database of ASDEX Upgrade plasmas with improved diagnostics for a variety of different plasma conditions has been analysed to study the momentum removal in the Scrape-Off Layer (SOL). A strong reduction, up to a factor of 100, of the electron pressure is observed close to the separatrix. Sets of L-mode and H-mode like plasma simulations with the SOLPS5.0 code package have supported the interpretation of the experimental observations (e.g., apparent momentum gain, strong radial position dependence) and helped to clarify the role of ion-neutral interactions. The experimental data are in turn used to check the SOLPS predictions, which differ quantitatively, suggesting that important pieces of physics are still not successfully captured by the code.

© 2017 The Authors. Published by Elsevier Ltd.

This is an open access article under the CC BY-NC-ND license.

(<http://creativecommons.org/licenses/by-nc-nd/4.0/>)

## 1. Introduction

Although momentum removal is considered a critical mechanism in obtaining and explaining plasma detachment, not much experimental work has been dedicated to its detailed study and comparison with up-to-date numerical predictions. In the Two-Point Model (TPM) [1], which assumes a stagnant plasma at up-stream position (e.g. mid-plane), sonic flow at the entrance of the sheath at the target and strong i-e thermal coupling ( $T_e = T_i$ ), the total pressure (static + dynamic) along the field lines is conserved when the target is considered as the only sink of momentum. Under these conditions, the momentum loss factor,  $f_{mom}$ , is given to be unity:

$$f_{mom} \equiv 2 p_{static,t} / p_{static,u} = 2 n_t T_t / n_u T_u = 1 \quad (1)$$

When additional sinks of momentum (e.g., interactions with neutrals, viscous transport and volume recombinations) are considered, and as the divertor temperature approaches 1 eV,  $f_{mom}$  is reduced to below unity.

A 1D analytical relation between the density at the entrance of the recycling region and the density at the target plate is given in

[2], under the assumption of isothermal flux tubes with a uniform neutral density. This result, in conjunction with the TPM, yields the Self-Ewald model:

$$f_{mom}(T_t) = 1 \left( \frac{\alpha}{\alpha + 1} \right)^{(\alpha+1)/2} \quad (2)$$

$$\alpha \equiv \langle \sigma v \rangle_i / (\langle \sigma v \rangle_i + \langle \sigma v \rangle_m)$$

where  $\langle \sigma v \rangle_i$  and  $\langle \sigma v \rangle_m$  are, respectively, the rate coefficients for ionization and momentum removal via charge exchange. At first approximation, these rates depend on the plate temperature only.

Previous studies of the electron pressure balance, primarily based on L-mode plasmas, for different tokamaks (C-mod [3,4], AUG [4,5], JET [6]) are qualitatively consistent with the Self-Ewald model. For C-mod, the parametric dependence of  $f_{mom}$  with  $T_{e,t}$  was found independent of the radial position of the flux tube in the SOL.

The present work has two objectives: (a) to extend the experimental AUG database from L-mode to H-mode with suitable data for the pressure loss analysis, encompassing a wide range of plasma parameters; and (b) to use SOLPS5.0 simulations for interpretation of the experimental results. With the current experimental settings, ion data in the SOL are not systematically available in ASDEX Upgrade. Therefore, as in previous studies, the electron densities and temperatures are used as a proxy for the total pres-

\* Corresponding author.

E-mail addresses: [ivan.paradela@ipp.mpg.de](mailto:ivan.paradela@ipp.mpg.de), [ivan.paradela@aalto.fi](mailto:ivan.paradela@aalto.fi), [ivanparadela@gmail.com](mailto:ivanparadela@gmail.com) (I. Paradel Pérez).

**Table 1**  
Range of characteristic parameters of the set of H-mode AUG discharges.

$B_t$ [T]	$I_p$ [MA]	$T_{e, \text{peak, targ}}$ [eV]
1.8 – 2.6	0.6 – 1.2	3.3 – 35.5
$P_{in}$ [MW]	$n_{e, \text{average}}$ [ $10^{19} \text{m}^{-3}$ ]	$q_{95}$
2.8 – 13.0	3.6 – 10.5	2.6 – 5.4

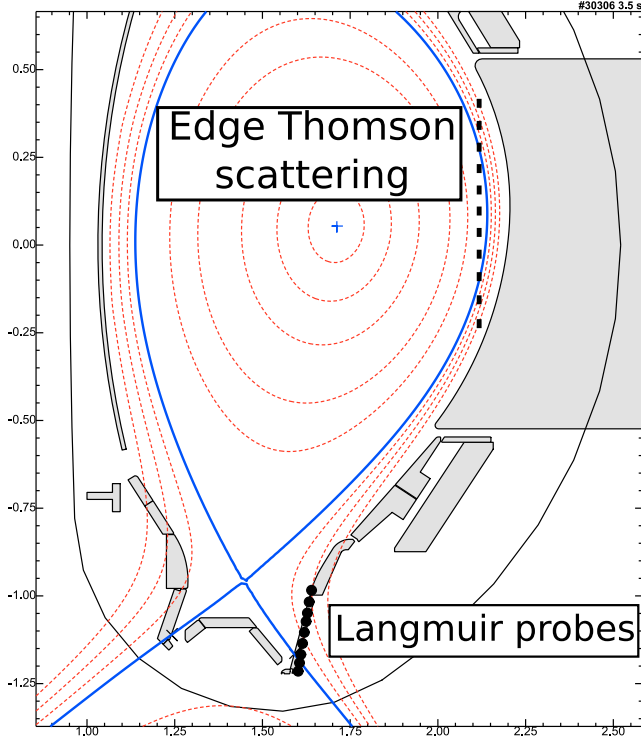


**Fig. 1.** Thomson scattering and Langmuir probes systems in AUG.

sure, assuming  $T_e = T_i$ . Herein,  $f_{mom}$  will refer to the electron momentum loss factor.

## 2. Methods and settings

### 2.1. Experimental setup

Measurements of the electron temperatures and densities at the low-field side mid-plane and LFS target for a set of 54 H-mode ASDEX-Upgrade plasmas have been used to estimate  $f_{mom}$  using Eq. (1). The set encompasses a wide range of plasma parameters and magnetic configurations, shown in Table 1, and it includes unseeded as well as nitrogen-seeded discharges. The set is limited to attached and partially detached discharges.

The analysed profiles are taken during inter-ELM phases of stationary plasmas. A single inter-ELM time window is defined by two boundaries: a minimum delay after the previous ELM and a time frame prior to the posterior ELM. The best fitting inter-ELM time window was manually selected for each plasma, usually between 3.5 and 1.5 ms before an ELM and 5 ms after the previous ELM. Electron upstream data of density and temperature were collected using the Vertical Thomson Scattering system, shown in Fig. 1. Only edge data were used to reconstruct the profile, since the main focus of the study involve the separatrix and the near SOL and local fits. Modified hyperbolic tangent (mtanh) is used as fitting model. The fit uncertainties are calculated from the covariance matrix.

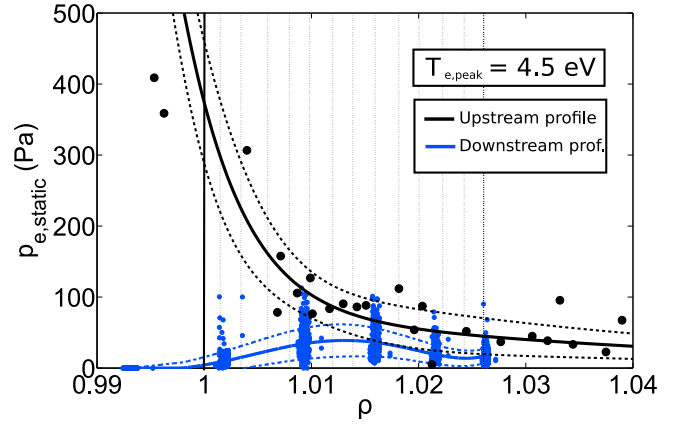


**Fig. 2.** Radial upstream and downstream pressure profiles. The dashed lines correspond to the fit uncertainties.

The electron density and temperature conditions were obtained by means of the triple Langmuir probes on the outer target (Fig. 1). Spline fitting is used to interpolate over the binned data. The experimental uncertainty was assessed statistically using the data gathered within the selected stationary time window. Because of the non-Gaussian nature of the Langmuir probes data (ELM screening, asymmetry of the distribution, etc), the median, instead of the average, is used and the considered uncertainty corresponds to the absolute deviation, instead of the standard deviation.

Examples of the radial upstream and downstream electron static pressure profiles are displayed in Fig. 2 for a low  $T_{e, t}$  case. The momentum loss factor,  $f_{mom}$ , is calculated in flux tubes with fixed radial locations, labelled by their distance from the separatrix measured at the outer mid-plane ( $\Delta s_{omp} = 1 \text{ mm}, 2 \text{ mm}, \text{etc.}$ ). Measurements were mapped to corresponding magnetic field lines using  $\rho_{pol}$ , a normalized flux parameter which assigns the value  $\rho_{pol} = 1$  to the separatrix and  $\rho_{pol} = 0$  to the magnetic axis.

The experimental reconstruction of the separatrix position is subject to an uncertainty of approximately  $\Delta s_{omp} \sim \pm 2 \text{ mm}$ . On the other hand, the upstream separatrix temperature is assumed to be rather insensitive to variation of other plasma parameters, as, according to the TPM,  $T_{u, u} \approx (7q_{||}/2\kappa_{0e})^{2/7}$  [1]. This, in conjunction with the experimentally observed strong gradient, leads to an alternative criterion for the separatrix position:  $T_{e, u}(\rho = 1) = 100 \text{ eV}$ . As in other experimental work, the upstream profiles were rigidly shifted with respect to EFIT (AUG standard equilibrium reconstruction) to match this criterion.

### 2.2. Setup of SOLPS simulations

H-mode [7] and L-mode-like [8]. plasma SOLPS5.0 simulations have been used for comparison to interpret the experimental data and to elucidate the dominant physical processes leading to momentum loss. Both sets of simulations correspond to attached and partially detached like plasmas. No impurity seeding has been used and the simulations were run without drifts. H-mode simulations were carried out with tungsten as the material of the plasma facing components but sputtering was not enabled. L-mode cases, due to their availability, simulated a full carbon machine with carbon sputtering. The divertor geometry was divllb [9] in all simulations. The atomic model specifications can be found in Table 2. For a subset of the L-mode-like simulations, elastic scattering between ions and molecules (Table 2, (B)) and/or charge exchange between ions and atoms (Table 2, (A)) were suppressed to study the role of the neutrals on momentum removal.

**Table 2**

Table of atomic model in SOLPS simulations. Carbon sputtering was only allowed in the L-mode-like cases.

Species	Type	Reaction
D	EI	$D + e \rightarrow D^+ + 2e$
	CX	$D + D^+ \rightarrow D^+ + D$ (A)
C (L-mode)	EI	$C + e \rightarrow C^+ + 2e$
	CX	$C + D^+ \rightarrow C^+ + D$
He	EI	$He + e \rightarrow He^+ + 2e$
	CX	$He + D^+ \rightarrow He^+ + D$
$D_2$	EI	$D_2 + e \rightarrow D_2^+ + 2e$
	DS	$D_2 + e \rightarrow D + D + e$
	DS	$D_2 + e \rightarrow D^+ + D + 2e$
	EL	$D_2 + D^+ \rightarrow D_2 + D^+$ (B)
$D_2^+$	DS	$D_2^+ + e \rightarrow D^+ + D^+ + 2e$
	DS	$D_2^+ + e \rightarrow D + D$
	DS	$D_2^+ + e \rightarrow D^+ + D + e$

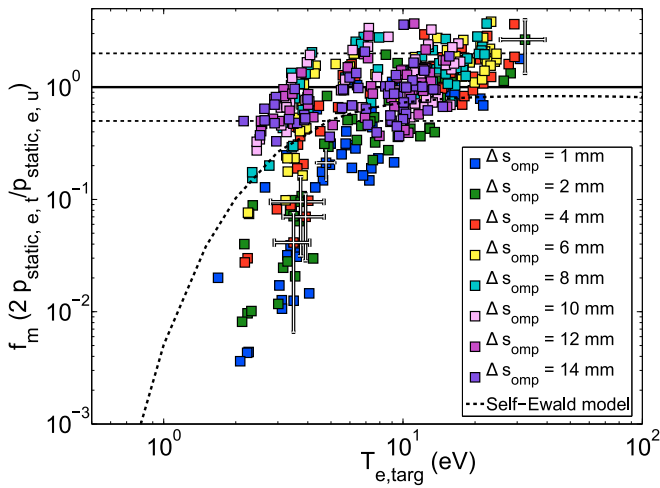


**Fig. 3.** Experimental electron momentum loss factor in ASDEX-Upgrade calculated in a number of flux tubes. The dashed line corresponds to the Self-Ewald model. The uncertainty in the measurements is indicated by the error bars.

### 3. Results

#### 3.1. Experimental results

At  $\Delta s_{omp} = 1$  mm, momentum losses for electrons are only observed for  $T_{e,t} < 10$  eV and they are stronger than predicted by the simple Self-Ewald model and the results of the aforementioned L-mode based studies for different machines [3–6] (Fig. 3). With increasing distance from the separatrix, momentum removal becomes increasingly less effective for the same values of  $T_{e,t}$ , in contradiction to the observations in C-mod. In the far SOL, temperatures below  $T_{e,t} \lesssim 3$  eV are required to observe significant losses. The results are qualitatively consistent with the momentum loss observed in the scarce H-mode plasmas with both steady state and transient neon seeding presented in [5], in which  $f_{mom}^{steady}$  (5 eV)  $\sim 0.1$  and  $f_{mom}^{transient}$  (1.5–3 eV)  $\sim 0.01 - 0.07$ , all of them measured at the flux tube corresponding to  $\Delta s_{omp} = \lambda_q \simeq 4$  mm.

For temperatures below a 2–3 eV, the accuracy of Langmuir probes on measuring the target temperature is significantly reduced. For instance, considering that  $T_{e,t}$  measurements were overestimated by 1 eV would align the evolution of  $f_{mom}(T_{e,t})$  with the prediction of the S-E model. Further studies employing other type of diagnostics with better low temperature resolution (e.g. spectroscopical measurements) are required to corroborate the dependence of  $f_{mom}$  on  $T_{e,t}$ . Despite the uncertainties, the results clearly

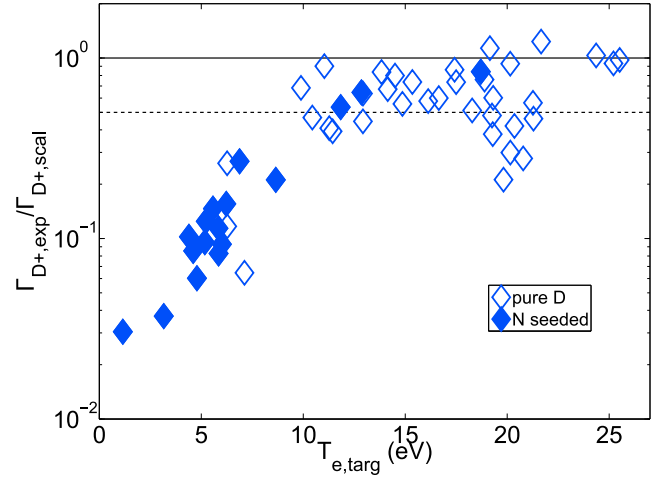


**Fig. 4.** Ion Flux Fraction at  $\Delta s_{omp} = 1$  mm as a function of the electron target temperature. The onset of detachment corresponds to  $T_{e,t} \sim 10$  eV, the same temperature below which strong momentum removal was observed. Additionally, no differences between unseeded and nitrogen-seeded plasmas for the same temperatures.

show a large momentum loss (factor of  $\sim 100$ ) near the separatrix already for partially detached plasmas (Fig. 3).

For  $T_{e,t} > 10$  eV, momentum is not only not removed, but an apparent electron momentum gain ( $f_{mom} > 1$ ) is observed Fig. 3. Apparent gains are also found in the flux tubes corresponding to the peak of the electron target temperature,  $T_{e,t, peak}$ , down to  $T_{e,t, peak} \sim 5$  eV, below which the profiles are flattened and the position of the peak becomes uncertain and could possibly be an artefact of the interpolation.

Momentum loss is considered to be closely connected to plasma detachment. Experimentally, detachment may be characterized by a reduction of the measured target ion flux compared to expectations, e.g. Degree of Detachment where  $\Gamma_{scal} = Cn^2$  [10]. This definition is, however, impractical for the present heterogeneous set of plasmas. Alternatively, the Ion Flux Fraction (IFF) is defined as:

$$IFF = \Gamma_{D^+}^{exp} / \Gamma_{D^+}^{scal} \quad (3)$$

$$\Gamma_{D^+}^{scal} = \frac{f_{pow} q_{||}}{\gamma e T_{e,t, targ}}$$

$$q_{||} = P_{SOL} / 4\pi R \lambda_q \theta_p, \quad \theta_p \approx \frac{2 \times 10^{-7} I_p}{a B_t}$$

where  $\Gamma_{D^+}^{exp}$  is the experimental ion flux to the target,  $\Gamma_{D^+}^{scal}$  is a simple theoretical expectation,  $q_{||}$  is the parallel momentum flux,  $\lambda_q$  is the power decay length calculated with the Eich scaling [11],  $\theta_p$  is the pitch angle and  $f_{pow} = q_t / q_{||}$  is the power loss factor which basically has the effect of rescaling the theoretical target ion flux. The value  $f_{pow} \sim 0.75$  is estimated from the fully attached, high  $T_{e,t}$  cases and kept constant for all the data set. In Fig. 4, the IFF at  $\Delta s_{omp} = 1$  mm is represented as a function of the electron target temperature. The onset of detachment, marked by a reduction of the experimental ion flux with respect to the theoretical scaling, corresponds to  $T_{e,t} \sim 10$  eV, below which also strong momentum removal is observed. This observation shows, as expected, that momentum and ion flux losses are closely linked. This important correlation, however, does not provide evidence of any causality relationship and both momentum and ion flux losses may be manifestation of the same underlying processes.

Finally, the results of the sensitivity scan are depicted in Fig. 5. When the upstream profiles were shifted by  $\delta s_{omp} = \pm 2.5$  mm, the differences are only quantitative, around  $\sim 50\%$  for the lowest temperatures. Using unshifted profiles (EFIT only) has a similar effect to displace the upstream profile towards the core, as usually

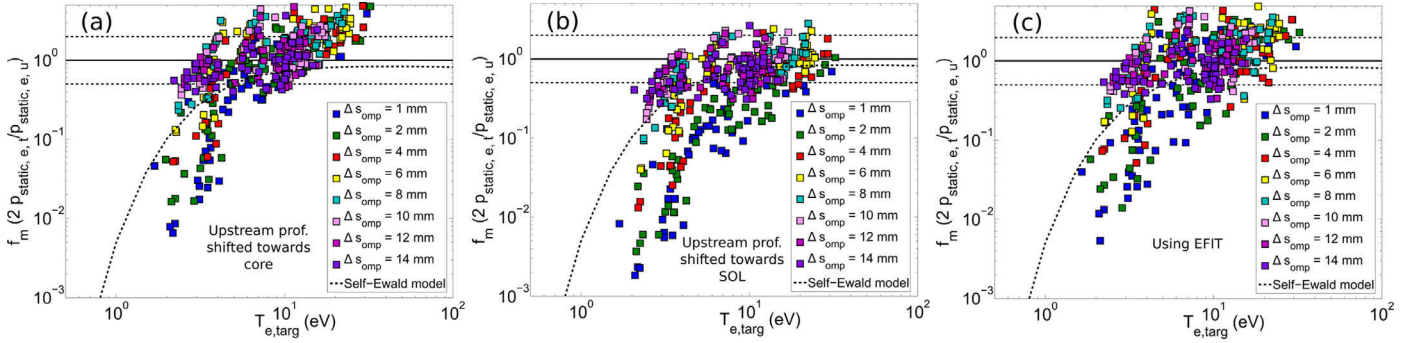


Fig. 5. Sensitivity scan performed by: (a,b) rigidly shifting the upstream profiles  $\delta s_{omp} = \pm 2.5$  mm and (c) using EFIT exclusively.

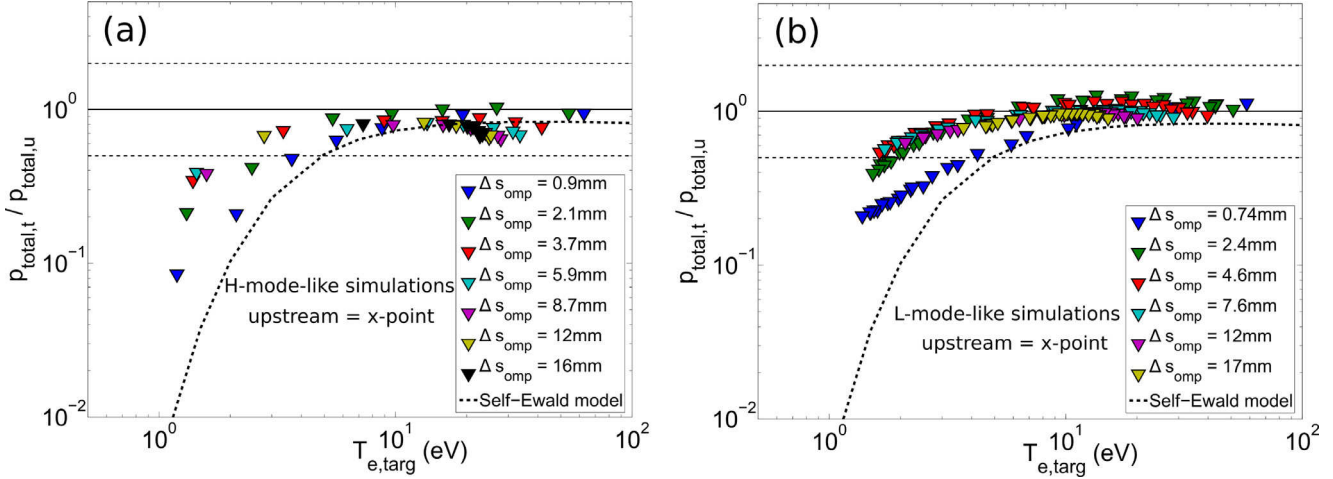


Fig. 6. Ratio of the downstream to upstream total pressure (total static + dynamic) as a function of the electron target temperature for (a) H-mode and (b) L-mode. The outer x-point is considered as the upstream position.

$T_{e,u,sep}^{EFIT} < 100$  eV, albeit the data seem more scattered, due to the large uncertainty in the separatrix position.

### 3.2. Simulations

Using SOLPS, it is possible to evaluate the total pressure ( $p_e + p_i + p_{dynamic}$ ) instead of assuming  $T_i = T_e$ , and the Bohm criterion, as in the experiment. The x-point is chosen as the upstream position since there no sources/sinks are expected from main plasma. The total pressure loss arises for  $T_{e,t} < 10$  eV in both H-mode and L-mode-like plasmas, as depicted in Fig. 6. Momentum removal is effective very close to the separatrix,  $\Delta s \sim 1 - 2$  mm, while no significant radial position dependence is observed further in the SOL. H-mode-like conditions are predicted to be slightly more effective in removing momentum with respect to L-mode-like cases, for the underline physics to be explored, while in both cases the momentum removal is less effective than what was found in experiments (around one order of magnitude in the near SOL) and the predictions of the SE model. However, the results are consistent with plasma simulations carried out with other codes, such as EDGE2D-EIRENE for JET [6], e.g.  $f_{mom}^{JET,C} \sim 0.3$ ,  $f_{mom}^{JET,ILW} \sim 0.35$ ,  $f_{mom}^{AUG,L-mode} \sim 0.3$  and  $f_{mom}^{AUG,H-mode} \sim 0.2$  at  $T_{e,t} \sim 2$  eV. Momentum is conserved for  $T_{e,t} > 10$  eV, as expected.

A notable caveat in the experimental study of momentum removal is that only  $T_e$  and  $n_e$  SOL data are readily available. Fig. 7 depicts the results of the SOLPS simulations using electron measurements exclusively. For  $T_{e,t} > 5$  eV, an apparent momentum gain is predicted, as observed in the experiment (Fig. 3). In the simulations, the low upstream density leads to low collisionality which in turn weakens the thermal coupling between ions and

electrons. The total upstream and target pressures are usually misestimated when using electron measurements only and assuming  $T_e = T_i$  in Eq. (1), since simulations predict that  $T_{i,u} > T_{e,u}$  and  $T_{i,t} < T_{e,t}$ . The relation  $T_{i,u} > T_{e,u}$  has been also observed experimentally [12,13]. The lack of ion measurements could then explain, at least partially, the apparent momentum gain observed in AUG experiments. For low temperatures,  $T_{e,t} < 5$  eV, when thermal equipartition is strong, the electron momentum loss factor corresponds with the total pressure removal observed for both H-mode and L-mode cases.

Another factor to take into consideration is the definition of the “upstream” poloidal position. In AUG, the Thomson Scattering data were collected closer to the OMP than to the x-point. Using the OMP as upstream position Fig. 7, the radial position dependence increases for high temperatures with large momentum gain in the near SOL. This effect is twofold: Within the section of the SOL connecting the OMP with the x-point, the main plasma provides a source for the near SOL while momentum is lost through the limits of the computational grid in the far SOL. This effect may help to explain the lack of radial position dependence reported in C-mod, since its upstream measurements are much closer to the x-point. Additionally, the collisionality is usually higher in C-mod than in AUG, and therefore the assumption  $T_i \approx T_e$  may hold.

#### 3.2.1. Role of ion-neutral interactions

When ion-neutral interactions are suppressed Fig. 8, the total momentum is conserved in the SOL across the entire target temperature range, down to  $T_{e,t} \sim 2$  eV, except in the vicinity of the separatrix. Following the momentum balance analysis in [14], Fig. 9 shows the different radial SOL pressure profiles as well



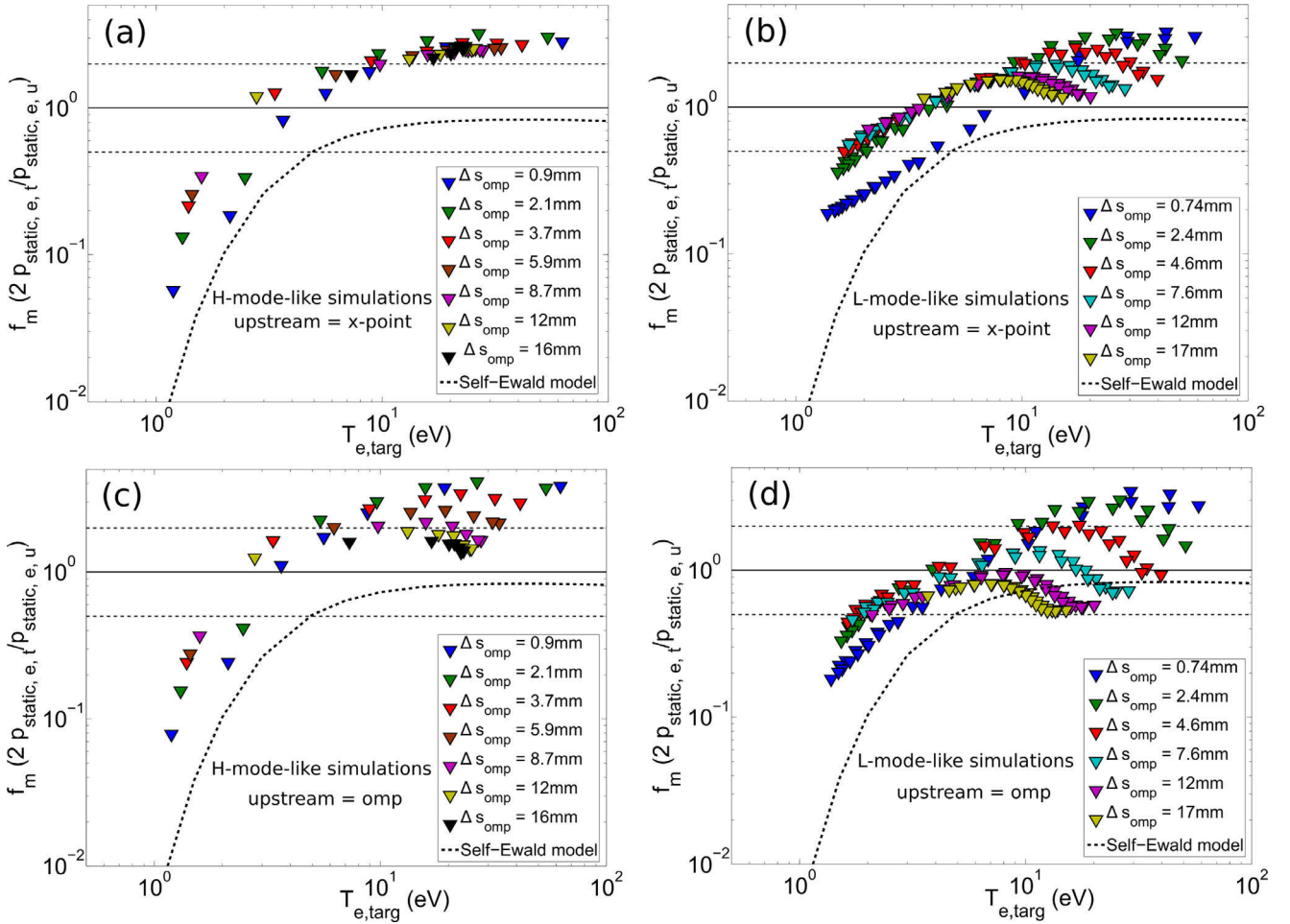


**Fig. 7.** Electron momentum loss factor as a function of the electron target temperature in (a,c) H-mode and (b,c) L-mode. The upstream position is defined as (a,b) the outer x-point and (c,d) the outer mid-plane.

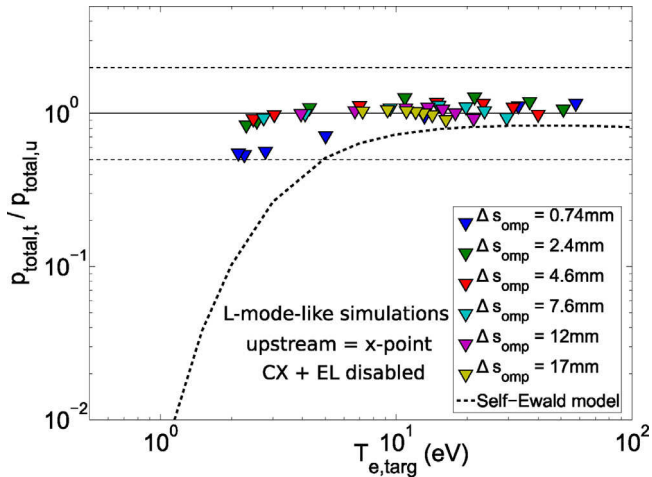


**Fig. 8.** Total pressure removal in cases in which charge exchange between atoms and ions and elastic scattering between molecules and ions were disabled. Some momentum is removed close to the separatrix mainly by transport.

as the integrated sources against the radial distance remapped to the OMP for the highest simulated upstream density (lowest  $T_{e,t}$ ), when both ion-atom charge exchange and ion-molecule elastic scattering are enabled, Fig. 9a, and disabled, Fig. 9b.

As expected, pressure is more efficiently removed when ions and neutrals are allowed to interact (CX+EL enabled, Fig. 9a). In

both scenarios, the downstream static pressure is roughly the same (within a factor of two in the closest points to the separatrix). The differences are caused by the change of the plate temperature, whereas the density profiles remain equal in both cases. Consequently, ion-neutral interactions reduce the dynamic pressure. When CX and EL are suppressed, diffusive transport is enhanced very close to the separatrix due to the steeper gradients of the non eroded profiles. Simulations in which only either CX or EL were allowed predict that CX accounts for most of the momentum removal due to neutrals and EL plays a very little role, Fig. 9c.

#### 4. Conclusions

An extensive H-mode plasma database with a variety of different plasma conditions has been used to evaluate parallel momentum removal in the SOL of ASDEX Upgrade. In the experiments, strong electron pressure losses are observed only for temperatures below  $T_{e,t} < 10\text{eV}$  near the separatrix ( $\Delta s_{omp} \leq 6\text{mm}$ ). For higher temperatures, an apparent momentum gain for electrons is found.

The SOLPS5.0 simulations underestimate the momentum removal with respect to the Self-Ewald model and the experimental results, thus suggesting that important pieces of physics are still not successfully captured by the code. However, they still serve as a useful tool to analyse the experimental results. They suggest that the apparent momentum gain observed in AUG is an artefact of the assumption  $T_i = T_e$ , which does not hold for high  $T_{e,t}$ . They reproduce the effect of the different poloidal reference locations for

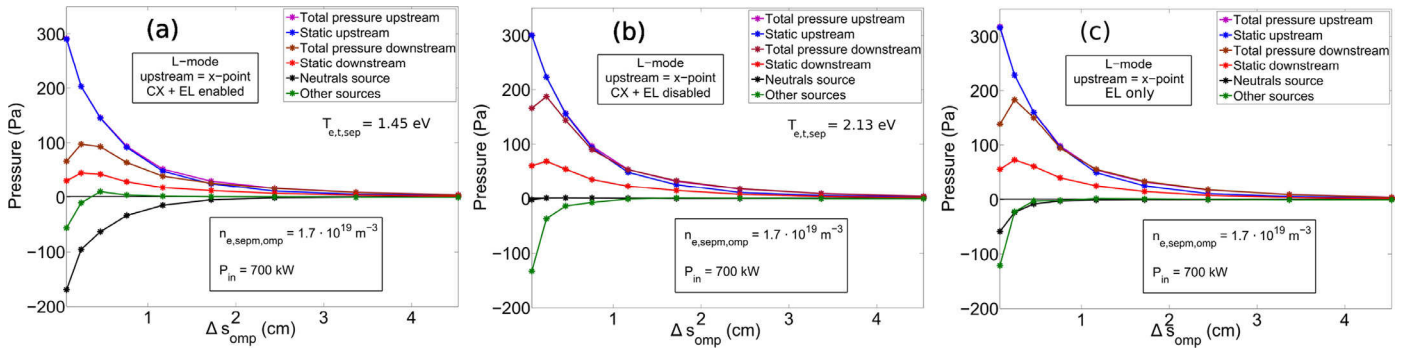


**Fig. 9.** SOLPS L-mode-like plasma pressure profiles mapped to the outer mid-plane with both charge exchange between ions and atoms (CX) and elastic scattering between molecules and ions (EL) (a) enabled, (b) with both disabled and (c) when only EL is included, for the case of highest simulated upstream density in all sets.

the upstream position, indicating that the disparities between AUG and C-mod observations (momentum gain and stronger radial position dependence) may be caused by the different collisionality regimes and upstream positions, therefore apparently reconciling the results.

Finally, they help to address the role of ion-neutral interactions. The importance of ion-atom charge exchange and ion-molecule elastic scattering was studied by switching them on/off in SOLPS. Charge exchange accounts for most of the momentum removal, whereas elastic scattering plays a very little role. The simulations show that charge exchange reduces the dynamic pressure.

#### Acknowledgement

The authors would like to thank David Moulton for providing the MATLAB routines used for the momentum balance analysis of the SOLPS5.0 simulations [15].

This work has been carried out within the framework of the EUROfusion Consortium and has received funding from the Euratom research and training programme 2014–2018 under grant

agreement No 633053. The views and opinions expressed herein do not necessarily reflect those of the European Commission.

This work has been supported by the Academy of Finland, grant n. 285143.

#### References

- [1] P.C. Stangeby, *The plasma boundary of magnetic fusion devices*, IOP, 2000.
- [2] S.A. Self, H.N. Ewald, *Phys. Fluids* 9 (1996) 2486–2492.
- [3] B. Lipschultz, et al., *Fusion Sci. Technol.* 51 (1996) 369–389.
- [4] C.S. Pitcher, et al., *Plasma Phys. Control. Fusion* 39 (1997) 779–930.
- [5] C.S. Pitcher, et al., *EPS Conf. on Plasma Physics and Controlled Fusion*, 1995.
- [6] C.G. Guilemaut, et al., *Nucl. Fusion* 54 (2014) 093012.
- [7] F. Reimold, et al., *J. Nucl. Mater.* 463 (2015) 128–134.
- [8] I. Paradelo Pérez, Master's thesis, Technische Universität München, 2014.
- [9] R. Neu, et al., *Nucl. Fusion* 43 (10) (2003) 1191.
- [10] A. Loarte, *Plasma Phys. Control. Fusion* 43 (2001) R183–R224.
- [11] T. Eich, et al., *Nucl. Fusion* 53 (9) (2013) 093031.
- [12] M. Kočan, *Plasma Phys. Control. Fusion* (2008).
- [13] D. Carralero, et al., *EPS Conf. on Plasma Physics and Controlled Fusion*, 2015.
- [14] V. Kotov, et al., *Plasma Phys. Control. Fusion* 51 (2009) 115002.
- [15] D. Moulton, 22nd Conference on Plasma Surface Interactions in Controlled Fusion Devices, poster n. P1.114, 2016.